Title

Ethanol internal reforming in solid oxide fuel cells: A path toward high performance metal-supported cells for vehicular applications

Authors

Dogdibegovic, Emir
Fukuyama, Yosuke
Tucker, Michael C

Publication Date

2020-02-01

DOI

10.1016/j.jpowsour.2019.227598

Peer reviewed

Ethanol internal reforming in solid oxide fuel cells: A path toward high performance metal-supported cells for vehicular applications

Emir Dogdibegovic[1,*], Yosuke Fukuyama[2], Michael C. Tucker[1,*]

[1]Lawrence Berkeley National Laboratory, Energy Storage and Distributed Resources Division, 1 Cyclotron Rd., MS 62-203, Berkeley, CA 94720, United States

[2] Nissan Motors Company, Ltd.; Nissan Research Center, EV System Laboratory, 1, Natsushima-cho, Yokosuka-shi, Kanagawa, 237-8523, Japan

*Corresponding authors:

Emir Dogdibegovic, Edogdibegovic@lbl.gov, Tel 1 (510)486-5635, Mail stop 62-R0203, 1 Cyclotron Road, Berkeley, CA 94720, United States

Michael C. Tucker, MCTucker@lbl.gov, Tel +1 (510)486-5304, Mail stop 62-R0203, 1 Cyclotron Road, Berkeley, CA 94720, United States

Abstract

Internal reforming of ethanol fuel was investigated on high-performance metal-supported solid oxide fuel cells (MS-SOFCs) with infiltrated catalysts. The hydrogen concentration and internal reforming effects were evaluated systematically with different fuels including: hydrogen, simulated reformate, anhydrous ethanol, ethanol water blend, and hydrogen-nitrogen mixtures. A simple infiltration of Ni reforming catalyst into 40 vol.% Ni-$Sm_{0.20}Ce_{0.80}O_{2-\delta}$ (Ni-$SDCN_{40}$) and fuel-side metal support leads to complete internal reforming, as confirmed by comparison to simulated reformate. The performance difference between hydrogen and fully-reformed ethanol is attributed entirely to decrease in hydrogen concentration. High peak power density was achieved for a range of conditions, for example 1.0 W cm^{-2} at 650 °C in ethanol-water blend, and

1.4 W cm^{-2} at 700 °C in anhydrous ethanol fuel. Initial durability tests with ethanol-water blend show promising stability for 100 hours at 700 °C and 0.7 V. Carbon is not deposited in the Ni-$SDCN_{40}$ anode during operation.

Keywords: Solid oxide fuel cell; Metal-support; Infiltration; Ethanol Internal Reforming

1. Introduction

Solid oxide fuel cells (SOFCs) need to satisfy three major criteria for commercialization in vehicular applications [1-7]: high performance and sufficient durability, start-up from cold to ~700 ºC within a few minutes to satisfy customer expectations, and low-cost fabrication of cell and stack materials. The symmetric-architecture metal supported solid oxide fuel cells (MS-SOFCs) [8-10] provide a number of advantages over anode or electrolyte-supported SOFCs (conventional SOFCs): they show excellent performance with hydrogen fuel (>1.5 W cm^{-2} at 700 ºC) [11], they are robust and have fast start-up capability [9, 12-16], they have excellent tolerance to thermal [17] and redox cycling [18, 19], and a single co-sintering step of porous ceramic backbones and a thin electrolyte between metal supports significantly reduce fabrication cost [8-10]. These properties of MS-SOFCs satisfy the major three criteria and are ideally suited for vehicular applications.

Currently, reforming of hydrocarbon fuels is mainly performed external to the SOFC stack. However, for small-scale and portable applications the complexity, size and weight of the system can be reduced by eliminating the external reformer and annex units [2], and performing internal reforming of the fuels inside the SOFC stack. This approach would be practical and cost-effective for vehicular applications due to size and weight restrictions for the SOFC system [1].

In this work, ethanol is considered as a renewable transportation fuel for use in MS-SOFC range extenders in vehicles. Dilution of ethanol with water increases safety, and is expected to suppress anode coking by increasing the steam-to-carbon ratio [1, 20].

Although liquid fuels are easier to handle and transport than hydrogen, their direct use in SOFCs can lead to decreased electrochemical activity, and anode deactivation due to carbon formation [21, 22], especially on the conventional Ni-YSZ (yttrium stabilized zirconia) anode. For the past few decades, internal reforming studies were conducted primarily with conventional SOFCs (no additional cell support is present, such as metal), predominantly using methane [23-28]. Direct utilization and internal reforming of liquid fuels including methanol [1, 29-32], ethanol [21, 33-37] and octane [38, 39] gained larger interest during the past decade due to global interest in improving energy efficiency of the transportation sector and reducing greenhouse gas emissions. Consequently, innovative coke-free anodes were developed for use with ethanol, however these materials are often less electrochemically active than Ni-YSZ.

To improve internal reforming of ethanol fuel in conventional SOFCs, the primary approach has been to augment or replace the Ni anode electrocatalyst. The most notable catalyst compositions can be classified into four categories: (1) Ni-based anodes such as Ni-YSZ [20, 40, 41], Ni-GDC [42, 43], Ni-CeO_2 [44, 45], Ni-CZO [46], Ni-BZCYYb [47], Ni-BZCY [22, 47], Ni-Al_2O_3[22], Ni-SrFeLaCoO3 [48], (2) Ni-free anodes including Cu-CGO [1, 41, 49], Cu-CeO_2 [50, 51], Cu-CZO [37], Cu-CeO_2-ScSZ [35, 52], Ir-CGO [44], Ru-CGO [1], Ru-Cu-CZO [1], Cu-Co(Ru)-CZO [53], Pd-LSCM [54], Ru-LSCM [55], (3) Ni-alloys with Sn [56], Fe [36, 48], Co [48, 57], and (4) Ni-free alloys such as CuZnAl [58], and CuCoRu [53]. The majority of these studies

reported low performance with ethanol (peak power <0.3 W cm^{-2} at 600-800 ºC), due to the use of inherently low-performing cells, incomplete reforming, or both.

Recently, notably improved performance with ethanol internal reforming has been reported. Shao et al. [22, 47] obtained peak power density (P_{max}) of 0.8 W cm^{-2} with Ni-BZCYYb anode at 700 ºC and 0.82 W at 700 ºC with Ni-Al_2O_3 reforming catalyst and pyridine added to the ethanol fuel. Virkar et al. [20] achieved 0.3 W cm^{-2} at 600 ºC and 0.8 W cm^{-2} at 800 ºC with Ni-YSZ anode. Arico et al. [48] obtained 0.6 W cm^{-2} at 800 ºC with Fe, Ni-alloy core-shell reforming catalyst. It is worth noting that Ni remains a major catalyst component for internal reforming of ethanol fuel. These studies suggest that obtaining P_{max} above 0.8 W cm^{-2} with ethanol fuel at the temperature range between 600-800 °C is challenging, which limits applications of conventional SOFCs. This can be ascribed, in part, to significant loss in catalytic activity with ethanol fuel when compared to operation with hydrogen, resulting in up to 50% loss in peak power density. Many literature reports on conventional SOFCs (in particular, anode-supported) also show severe mass transport limitation for ethanol, observed as a limiting current density that is not seen when operated in hydrogen fuel [1, 48, 50]. Presumably, this is due to hydrogen concentration polarization arising from the density and thickness of the anode support and low hydrogen concentration in the reformed fuel.

It is also imperative to note that a simple comparison of SOFC performance with hydrogen and ethanol fuel is commonly reported in literature. Such approach does not address the large range of derating factors. Individual effects that should all be taken into consideration include: (1) hydrogen concentration (lower hydrogen content in reformed fuel and concentration polarization

across the thickness of the anode), (2) internal reforming (chemical catalytic activity towards fuel reforming), and (3) coking (deposition of solid carbon that can block the reforming or electrochemical catalysts active sites). Separation of these effects would inform development of cell architecture and catalyst compositions for ethanol internal reforming.

In this work, we isolate the impact of electrocatalytic, internal reforming, hydrogen concentration, mass transport, and coking limitations in button cells under low fuel utilization. We anticipate that this approach can be easily extended to operation with many other fuels of interest, and will accelerate development of high-performance cells with internal reforming. Electrocatalytic performance of the cell is established with hydrogen fuel as a baseline. To assess the impact of internal reforming, performance is compared for hydrogen, ethanol internal reforming, and simulated reformate which represents the anode gas composition in the case of complete internal reforming. To isolate hydrogen concentration effects, hydrogen/nitrogen mixtures representing the hydrogen concentration expected for complete internal reforming were used. To separate reforming and mass transport limitation, the cell area specific resistance (ASR) is compared at high and low operating potential. To eliminate coking effects, ethanol-water mixtures with steam-to-carbon (SC) ratio above the thermodynamic limit for coking were employed.

Identifying internal reforming as the dominant limitation for MS-SOFCs enables targeted improvement efforts for the reforming catalyst. Infiltration of various reforming catalysts over 40 vol.% Ni-$Sm_{0.20}Ce_{0.80}O_{2-\delta}$ ($SDCN_{40}$) anode and fuel-side metal support was employed to improve chemical reforming activity and promote in situ fuel processing. Dramatically improved

performance with ethanol internal reforming is achieved, demonstrating that MS-SOFCs are promising for high-performance range extenders in vehicular applications.

2. Experimental

2.1 Cell fabrication

Detailed cell fabrication has been described in our previous work [11, 59]. In brief, the green cells were prepared by tape-casting and lamination of individual scandia-ceria-stabilized zirconia (10Sc1CeSZ, DKKK, Japan) electrode backbone and electrolyte layers, and stainless steel (P434L alloy, water atomized, Ametek Specialty Metal Products) support layers. The pores were introduced to ceramic backbones and metal support layers with polymethyl methacrylate poreformer beads (Esprix Technologies). Laminated cells were then laser-cut (Hobby model, Full Spectrum Laser) and debinded in air at 525 °C for 1h with 0.5 °C min^{-1} heating rate. The cells were then sintered at 1350 °C for 2h in a tubular furnace with flowing 2% hydrogen/argon. The resulting cells were 30 mm in diameter, had 12 μm thick electrolyte, 25 μm thick porous cathode and anode backbones, and 250 μm thick porous metal supports.

2.2 Catalyst precursors and cell infiltration

Metal nitrates (Sigma Aldrich) were mixed with Triton-X 100 (Sigma Aldrich) with loading of 0.3 g per 2 g of resulting catalyst and dissolved in 20 to 100 wt.% (vs. catalyst) of water. More detailed description can be found in our previous reports [11, 59]. The cells were then infiltrated with precursor mixture of metal nitrates using vacuum. Acrylic paint mask (Liquitex) was used to cover the cell edges, providing 1 cm^2 cathode active area, while the anode was fully covered with the catalyst. The cells were then fired at 3 °C min^{-1} heating rate to 600 °C or 850 °C for 30

min in air to convert the precursors to the intended oxide phases [59]. Pr_6O_{11} (PrOx) cathode catalyst was infiltrated a total of three times, and $SDCN_{40}$ anode catalyst was infiltrated four times [11]. Reforming catalyst precursors (Ni, Cu, or Ru-nitrate) were applied on the anode side (previously infiltrated with $SDCN_{40}$) via vacuum infiltration and firing at 550 °C for 0.5 h. The precursors were diluted with water in 1:2.5 mass ratio. Alternatively, cells with concentrated Ni nitrate solution (2:1 mass dilution with water) were infiltrated twice and fired after each infiltration at 550 °C for 0.5 h.

2.3 Cell testing

A button cell rigs fabricated from alumina or 410 stainless steel were equipped with two K-type thermocouples placed ~2 mm from the cell's surface on air and fuel sides. The anode thermocouple was placed 1 mm from fuel inlet. Both sides of the cell were spot-welded with a small Pt mesh carrying two NiCr wires, providing four probe measurements. Cells were sealed with GM31107 glass paste (Schott, Germany), then heated to 200 °C at 2 °C min^{-1} and to 700 °C at 10 °C min^{-1} with 1 h hold. The anode chamber was then flushed with nitrogen followed by 3% humidified hydrogen. Simulated reformate fuel was a customized gas mixture (52.3 mol.% hydrogen, 25 mol.% water, 11.8 mol.% carbon monoxide, 9.9 mol.% carbon dioxide, and 1 mol.% methane) (Praxair). Liquid fuel (anhydrous ethanol, or 45 vol.% ethanol/ 55 vol.% water) was then delivered to the cell with a syringe pump (New Era, NE-1000x) at a flow rate of 10 µL min^{-1}, through a pre-heated fuel line. The cathode was exposed to static air. The i-V and electrochemical impedance spectroscopy (EIS) measurements were recorded with a VMP3 multichannel potentiostat and current booster (Biologic).

2.4 ASR Analysis

The literature cell ASR at a specific voltage was extrapolated from the corresponding i-V curves using WebPlotDigitizer [60] software and the local derivative of the i-V curve. For instance, each i-V plot from the literature was fed into WebPlotDigitizer software and the i-V curve of interest was traced to generate the raw data. The corresponding i-V curve was then fit with a fifth order polynomial in Excel. The first derivative of the polynomial equation provided the cell ASR at a specific voltage.

2.5 Cell Characterization

Post-mortem analysis on cells was conducted with Zeiss Gemini Supra 55 VP-SEM scanning electron microscope (SEM) with built-in energy-dispersive X-ray spectrometer (EDS).

3. Results and Discussion

When operated with direct internal reforming of ethanol fuel, the cell performance is limited by the OCV (which is primarily affected by hydrogen concentration at the anode and is difficult to improve for a given fuel and steam content), electrochemical ASR (cathode, electrolyte and anode) which can be measured in hydrogen, incomplete reforming (which can be addressed by improving the reforming catalyst), coking (which can be addressed by fuel steam content and catalyst composition), and mass transport limitation (which can be addressed by anode structural modifications). The approach taken in this work is to elucidate ethanol internal reforming performance in button cells, and identify the dominant limitation(s) through a detailed analysis of performance with various fuels. Identifying the critical limitations then informs efforts to further improve performance.

3.1 Diagnosis of performance, hydrogen concentration and reforming effects

A MS-SOFC with PrO_x/SCSZ/$SDCN_{40}$ configuration was tested at 700 °C with various fuels to diagnose operation with ethanol internal reforming. Two baseline fuels were used for comparison: hydrogen (3% humidified), and simulated reformate with the thermodynamic gas mixture composition calculated for completely reformed 45 vol.% ethanol-55 vol.% water (0.65:1 mass ratio) blend at 700 °C [61]. The strategic choice for ethanol-water blend over anhydrous ethanol fuel is based on three major factors: (1) the blend can eliminate the need for water recirculation systems in vehicles, (2) ethanol dilution with water is safer, and (3) the resulting steam-to-carbon ratio is outside the carbon formation region at 700 °C [61], which is further discussed in *Section 3.4*. Thermodynamically, carbon formation is not favorable until ethanol: water mass ratio of 1.61:1 (700 °C) or 1.28:1 (650 °C) is exceeded [61]. Therefore, only the simulated reformate for ethanol-water blend was considered in this work.

The cell displays high performance with humidified hydrogen, 1.62 W cm^{-2}, **Fig. 1a**. When switching to simulated reformate, peak power density (P_{max}) drops to 1.44 W cm^{-2}. This decrease is due to hydrogen concentration effects, primarily the reduced OCV, confirmed by using a diluted-hydrogen fuel (52.3 mol.% hydrogen in nitrogen) with the same hydrogen concentration as the simulated reformate. The resulting performance (P_{max}= 1.40 W cm^{-2}), **Fig 1b,** is in agreement with that for simulated reformate. The performance for direct internal reforming of ethanol-water blend (P_{max} = 0.87 W cm^{-2}) is significantly lower than for simulated reformate, suggesting a significant additional limitation associated with reforming of the liquid fuel, **Fig. 1a**.A similar trend is observed for anhydrous ethanol at 700 °C: for the diluted hydrogen

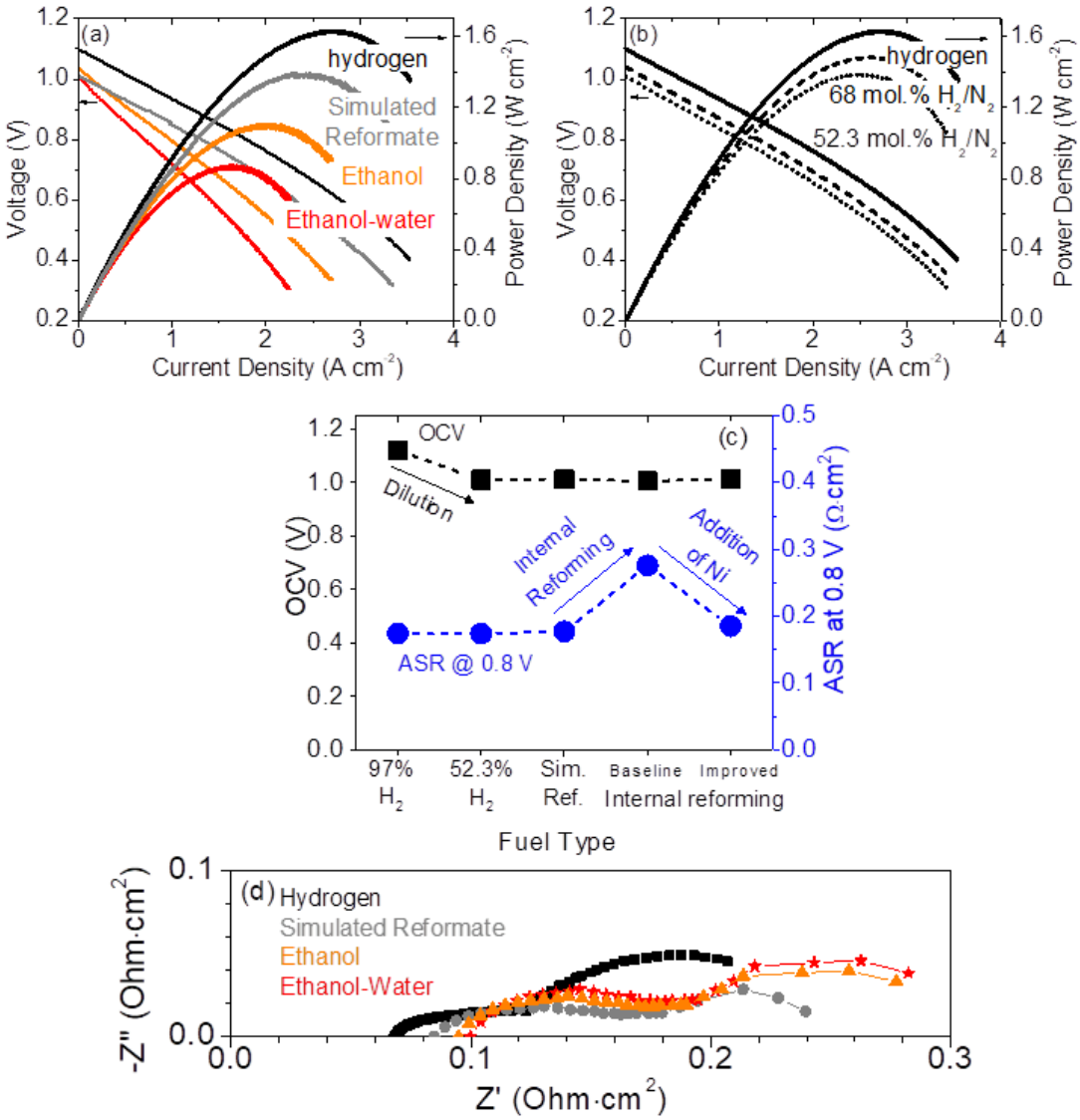

Figure 1. Assessment of ethanol internal reforming in MS-SOFCs at 700 °C. Polarization and power density for (a) various fuels and (b) hydrogen-nitrogen mixtures equivalent to hydrogen concentration in fully-reformed dry ethanol and ethanol-water blend. (c) OCV and ASR (at 0.8 V) for hydrogen and ethanol-water blend fuels (reformate equivalent H_2/N_2 mix, simulated reformate, and direct internal reforming for baseline and improved reforming catalysts). (d) EIS spectra at OCV for hydrogen (squares), simulated reformate (circles), ethanol (triangles), and ethanol-water blend (stars).

concentration expected for complete reforming (68 mol.%) [61], P_{max} of 1.47 W cm^{-2} is achieved, but for direct internal reforming P_{max} is 1.1 W cm^{-2}, which is consistent with analogous comparison made by Borchiellini et al. [62]. If the liquid fuel is fully reformed to the equilibrium composition in the metal support, it would provide the same performance and OCV as the simulated reformate. We surmise that coking is not a significant contributor to the performance limitation for direct internal reforming here because the steam-to-carbon ratio for simulated reformate and ethanol-water blend is outside the thermodynamic coking region. Furthermore, if coking was prevalent, it would be worse for anhydrous ethanol which has a lower steam-to-carbon ratio than ethanol-water blend, yet the performance for anhydrous ethanol is higher. Electrochemical durability and coking is discussed in more detail in *Section 3.4*.

The performance decrease observed for internal reforming can be deconvoluted into contributions from decrease in concentration of electrochemically-active species, which affects the open circuit voltage (OCV), and internal reforming, which impacts the cell area-specific resistance (ASR). This is illustrated in **Fig. 1c**, with ASR calculated from local derivatives of the respective i-V curves at 0.8 V. The hydrogen concentration effect is prominent when switching from pure hydrogen to lower hydrogen concentration (hydrogen-nitrogen mixture) and simulated reformate (52.3 mol.% hydrogen), while ethanol-water blend provides similar hydrogen concentration and therefore shows similar OCV with simulated reformate. Theoretical OCV is 1.12 V for 3% H_2O/H_2, 1.02 V for simulated reformate and 52 mol. % H_2/N_2, and 1.04 V for 68 mol.% H_2/N_2. The small decrease in OCV (100 mV drop when compared to hydrogen) is a strong indication of indirect electro-catalytic oxidation of ethanol over $SDCN_{40}$ anode [22], in which ethanol chemically decomposes to reformate, and then H_2, CO, and CH_4 are further

electrochemically oxidized to generate electricity. Measured OCV is very similar for all fuels other than 97% H_2-3%H_2O, suggesting reforming is essentially complete [63].

When a cell is operated in reformate, the electrochemical reaction is rapid and is not limiting the cell performance, as evident by no change in ASR, **Fig. 1c**. When operated with internal reforming of liquid fuel, however, the performance is significantly lower and ASR increases. The ASR is dominated by reforming effects, and not significantly impacted by hydrogen concentration as seen by comparing ASR for pure hydrogen, hydrogen-nitrogen mixture, and simulated reformate. The ASR increases dramatically when switching from simulated reformate to internal reforming of liquid fuel. Various possibilities could account for this, including competition between reforming and electrochemical reactions on the Ni in the active anode layer, or slow kinetics in the complicated multi-reaction reforming pathway that may include the water-gas shift reaction or electrochemical oxidation of CO. With addition of Ni surface area, further discussed in *Section 3.2*, the cell ASR was again comparable to simulated reformate.

It should be noted that the slight mass transport limitation observed in all polarization curves below about 0.5 V is due to oxygen diffusion in the cathode, and is unrelated to changes in the fuel composition. This was demonstrated previously by comparing polarization with air and oxygen [11]. Since MS-SOFCs have a highly porous structure [11, 64] the concentration polarization across the thickness of the anode is expected to be negligible and have none or minimal impact on the cell ASR. This is often not the case for thick and dense anode supported cells (ASCs) which show severe mass transport limitation [1, 48, 50] for ethanol (although not

observed in hydrogen fuel). The ASR at high current (low voltage) is further increased by mass transport restriction arising from resistance to diffusion in the anode due to anode layer thickness, density or tortuosity. The ASR at low voltage (e.g. 0.4 V) can be separated into three portions: (1) electrochemical, which is approximately the ASR at 0. 8 V in hydrogen, (2) additional limitation due to reforming, which is roughly the ASR difference between hydrogen and ethanol at 0.8 V, and (3) mass transport, which is the additional ASR at low voltage. Using this approach, the individual ASR contributions for MS-SOFCs and ASCs can be estimated. For the selected literature reports, the anode mass transport limitation in ASCs dominates the cell ASR at 0.4 V, **Table 1**. The anode mass transport restriction also contributes significantly to loss in P_{max} in ASCs (occurring at or near low voltage), while the ASR changes at high voltage are less evident. For instance, Virkar et al. [20] measured ~50% decrease in P_{max} with ethanol-water blend (50:50 by volume) at 800 °C; Liu et al. [22] measured ~30% decrease in P_{max} with steam reforming of anhydrous ethanol at 700 °C; and Shao et al. [47] measured ~16% P_{max} loss with anhydrous ethanol fuel.

Table 1. Individual ASR contributions for a Ni2x MS-SOFC (700 °C) in this work and a few selected conventional SOFCs (800 °C) operated in ethanol fuel at 0.4 V.

Reference	**$ASR_{0.4V}$ ($\Omega \cdot cm^2$)**			
	Total	**Electrochemical**	**Reforming**	**Anode Mass Transport**
This work	0.26	0.18	$8.20 \cdot 10^{-3}$	0*
[50]	1.31	0.48	0.22	0.61
[1]	4.97	0.54	0.75	3.68
[48]	9.74	0.26	0.90	8.58

*Cathode mass transport accounts for the remaining ASR [11].

Further insight is provided by electrochemical impedance spectroscopy, **Fig 1d**. The significant decrease in power output observed with internal reforming of liquid fuels is dominated by catalytic activity of $SDCN_{40}$, appearing as a large increase in electrode polarization resistance (R_{pol}). This increase originates solely from the anode, since a single cell was operated isothermally in different fuels. A smaller increase in ohmic resistance (R_{ohm}) when switching from hydrogen to reformate and liquid fuels is attributed to two separate mechanisms. The oxygen partial pressure (pO_2) in the anode increased from 10^{-24} in 3% humidified hydrogen to 10^{-23} in anhydrous ethanol and 10^{-22} in ethanol-water blend [61], which may lead to decrease in total conductivity of samaria-doped ceria (SDC). Haile et al. [65] showed mixed electronic and ionic conductivity arising at low pO_2, between 10^{-20} to 10^{-25}, for nanostructured SDC. In this pO_2 region, ionic and electronic conduction mechanisms compete, and total conductivity decreases with increasing pO_2. We expect this mechanism also occurs for the $SDCN_{40}$ anode. Secondly, endothermic reactions in the anode chamber lead to a small temperature drop, measured to be < 3 °C at the anode, which could have contributed to increased R_{ohm}.

3.2 Screening of reforming catalysts

Internal reforming of ethanol in conventional SOFCs showed the highest performance for Ni-based reforming catalysts [20, 22, 47, 48]. In some cases Cu or Ru-based catalysts also showed promise including: Cu-CGO [1, 37, 41], Cu-CeO_2 [50, 51], Cu-CeO_2-ScSZ [52], Ru-CGO[1], Ru-Cu-CZO [1], Cu-Co(Ru)-CZO [53], Cu-CZO [37], and Ru-LSCM [55]. We therefore screened Ni, Cu, and Ru for internal reforming of ethanol fuel in MS-SOFCs. The highly porous MS-SOFC structure allows for a simple infiltration of reforming catalysts on top of the existing $SDCN_{40}$ anode catalyst, which is effective for electrochemical oxidation of hydrogen (1.6 W cm^{-}

^{2} at 700 °C), **Fig. 1a**. Rather than modifying the bulk anode composition as is often done in anode-supported SOFCs, here the fuel-side metal support and electrode backbone were infiltrated with additional reforming catalyst. The ASR at 0.8 V in ethanol-water blend was gradually decreased from 0.276 Ω·cm^2 to 0.185 Ω·cm^2 at 700 °C with additional Ni loadings on the anode, **Table 2**. ASR increased with Cu and Ru catalysts. It is possible that Cu and Ru blocked active Ni sites. Based on these findings, 2xNi-SDCN$_{40}$ was selected as the primary candidate for improving performance when internally reforming ethanol in MS-SOFCs.

Table 2. Screening of reforming catalysts at 700 °C in ethanol-water blend.

	SDCN$_{40}$	**Ni-SDCN$_{40}$**	**2xNi-SDCN$_{40}$**	**Ru-SDCN$_{40}$**	**Cu-SDCN$_{40}$**
OCV (V)	1.01	1.01	1.02	1.01	1.01
ASR$_{0.8\ V}$ (Ω·cm^2)	0.28	0.23	0.19	0.49	0.66

3.3 Improved performance with ethanol internal reforming

Infiltration of Ni to the SDCN$_{40}$ anode increased P_{max} from 0.8 W cm^{-2} to 1.16 W cm^{-2} at 700 °C, **Figure 2a**. An additional infiltration further increased P_{max} to 1.32 W cm^{-2}, which is very similar to the performance with simulated reformate, indicating complete internal reforming and sufficient Ni surface area available for electrochemical oxidation of hydrogen and carbon monoxide. Operation with 2xNi-SDCN$_{40}$ anode at 650 °C also shows high performance, **Fig. 2b**. However, there is a significant decrease in P_{max} from 1.32 W cm^{-2} to 1.0 W cm^{-2} for ethanol-water blend associated with the 50 °C reduction in operating temperature. This decrease is 10% larger than the P_{max} difference for hydrogen at the same temperatures, which suggests that the reforming limitation is more thermally activated than the electrochemical processes present in

this cell design. Reforming of anhydrous ethanol fuel shows higher P_{max} (1.4 W cm^{-2} at 700 °C, and 1.1 W cm^{-2} at 650 °C) when compared to ethanol-water blend.

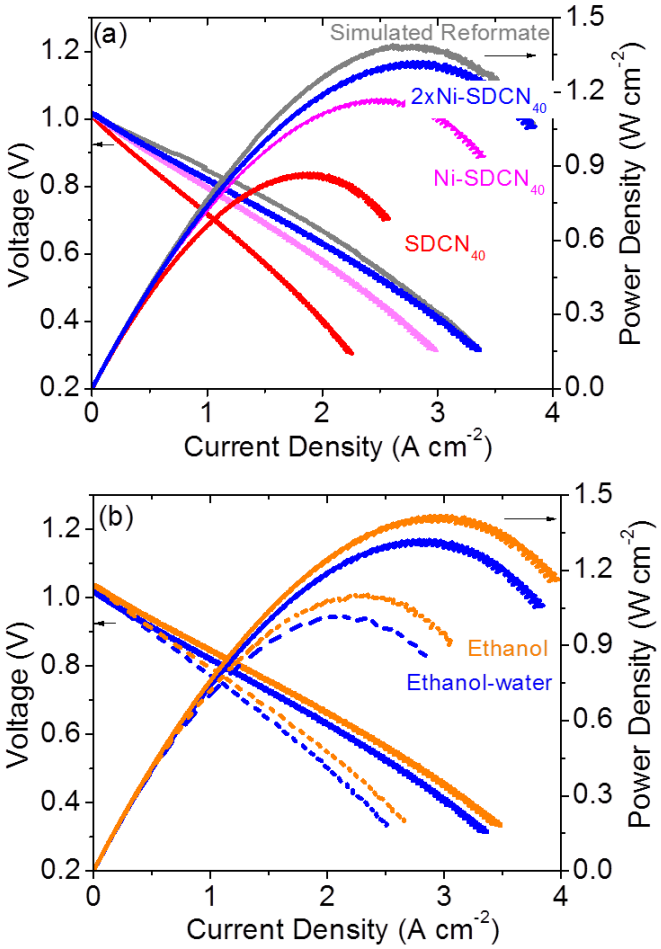

Figure 2. Ethanol internal reforming with Ni-$SDCN_{40}$ anode. (a) Polarization and power density with ethanol-water blend at 700 °C with $SDCN_{40}$, Ni-$SDCN_{40}$, and 2xNi-$SDCN_{40}$ anodes, compared to simulated reformate with $SDCN_{40}$. (b) Performance with anhydrous ethanol and ethanol-water blend at 650 °C (dashed lines) and 700 °C (lines) with 2xNi-$SDCN_{40}$ anode.

Ethanol internal reforming performance for an improved MS-SOFC is compared to literature reports that demonstrated high P_{max} for various anode catalysts in **Fig. 3**. The MS-SOFC performance is almost twice that of the best conventional SOFCs. The improved performance of

MS-SOFCs in this work is not necessarily from reforming progress alone but could also be a result of recent cathode, electrolyte, anode, and cell structure development. The highest P_{max} in conventional SOFCs was obtained with Ni-based catalysts [6, 20, 40, 46, 47, 66], consistent with the results in *Section 3.2*, and significantly lower P_{max} was reported for Ni-free anodes [1, 6, 35, 37, 50, 53, 67]. The majority of previous studies on conventional SOFCs were conducted at 800 °C to promote internal reforming and enhance catalytic activity, yet showed low ethanol internal reforming performance (P_{max} < 0.3 W cm^{-2}) and therefore are not included in this comparison.

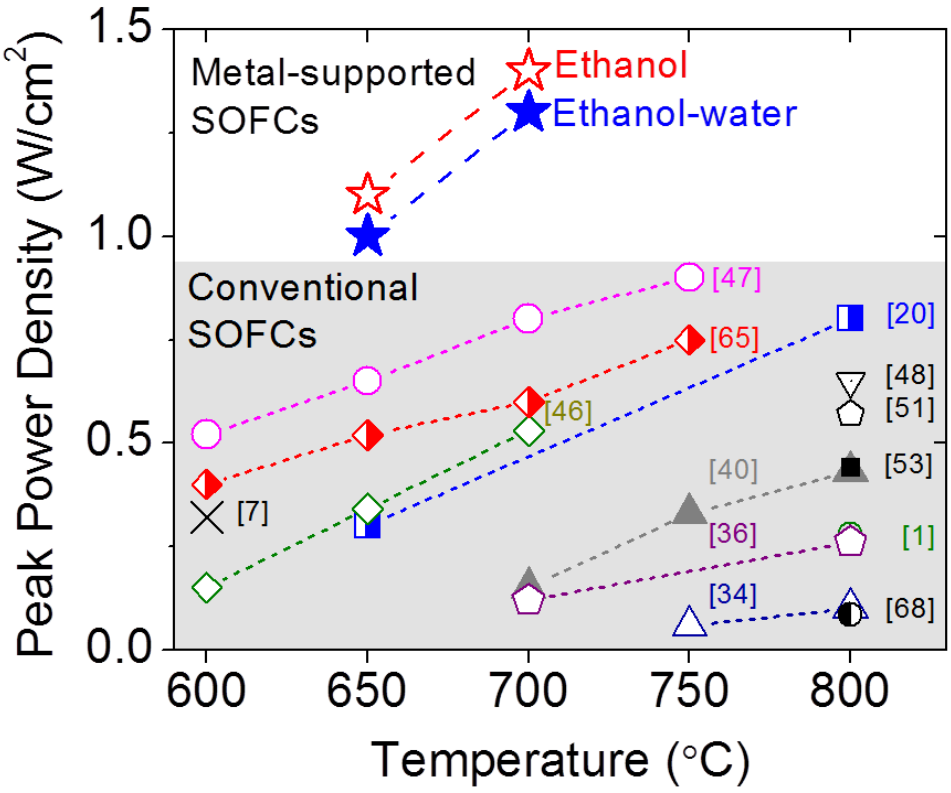

Figure 3. Comparison of cell performance under ethanol internal reforming conditons. (Bottom grey region) Summary of previous performance of conventional SOFCs with internal reforming of ethanol fuel (dry or steam reforming). (Top white region) Performance obtained in present work for MS-SOFCs with 2xNi-$SDCN_{40}$ anode operating with anhydrous ethanol (red) and ethanol-water blend (blue).

3.4 Durability

Retaining good durability of MS-SOFCs with internal reforming of ethanol is a crucial factor for commercialization of the technology for vehicular applications. The operating temperature between 650 and 700 °C is preferred due to a suitable tradeoff between performance and longevity [11, 64]. However, operation with carbon containing fuels often leads to coke formation [21, 22]. Nickel cermets, which are the state-of-the-art anode materials for SOFCs, exhibit excellent activity for hydrogen electro-catalytic oxidation and high electrical conductivity; however, they also catalyze the pyrolysis of hydrocarbons and oxygenated hydrocarbons [22]. Thus, rapid and irreversible deterioration in performance often occurs when the cells operate on carbon-containing fuels because of significant coke formation over the nickel anode surface. Based on the thermodynamics of solid carbon formation, higher operating temperature [51, 68] and appropriate steam content were shown to alleviate coking [20, 22, 47, 48, 50]. However, operation at elevated temperatures (T > 700 °C) can often lead to shorter lifetime due to faster material degradation (microstructural changes, elemental inter-diffusion between cell components, catalyst phase degradation), accelerated chromium poisoning, and increased oxidation of stainless steel-based interconnectors. Therefore a main focus of previous work is development of reforming catalysts that enable reduced operating temperature.

In this work 2xNi-SDCN$_{40}$ anode showed the highest P_{max} in the temperature range of 650 to 700 °C and was selected for durability studies with ethanol fuel. Based on thermodynamic calculations [61], ethanol diluted with 55 vol.% water (equivalent to ethanol: water mass ratio of 0.65:1) is expected to be free of carbon formation above 160 °C, where 160 °C is the calculated temperature below which coking occurs. In our previous work [64], we developed MS-SOFCs

that exhibit stable electrochemical operation in hydrogen with 2.3 % kh^{-1} degradation. Durability improvement was achieved through chromium suppression and electrocatalyst microstructure stabilization. The 2xNi-$SDCN_{40}$ anode was implemented with these improved cells and the 100 h durability tests at 700 °C and 0.7 V in 3% humidified hydrogen and ethanol-water blend are shown in **Fig. 4**. Stable electrochemical operation in ethanol-water blend was obtained from 25 to 100 hours at 700 °C and 0.7 V. The initial transient behavior with ethanol fuel might be attributed to de-activation of the reforming catalyst. Post-mortem SEM analysis on cells operated in different fuels confirmed the absence of carbon, and the anode microstructure remained unchanged, **Fig. 5a-b**. EDS analysis throughout the anode bulk and near the anode-electrolyte interface did not show any significant carbon deposition, consistent with complete internal reforming of ethanol-water blend to the products expected from thermodynamic calculation.

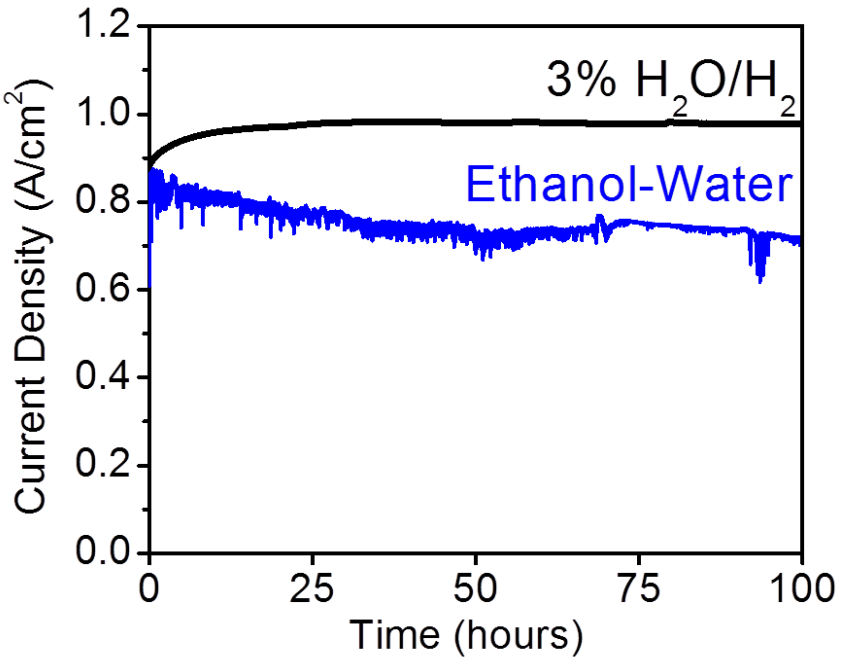

Figure 4. Initial durability with ethanol internal reforming. Durability at 700 °C and 0.7 V with 2xNi-$SDCN_{40}$ anode operating with 3% humidified hydrogen (black) and ethanol-water blend (blue).

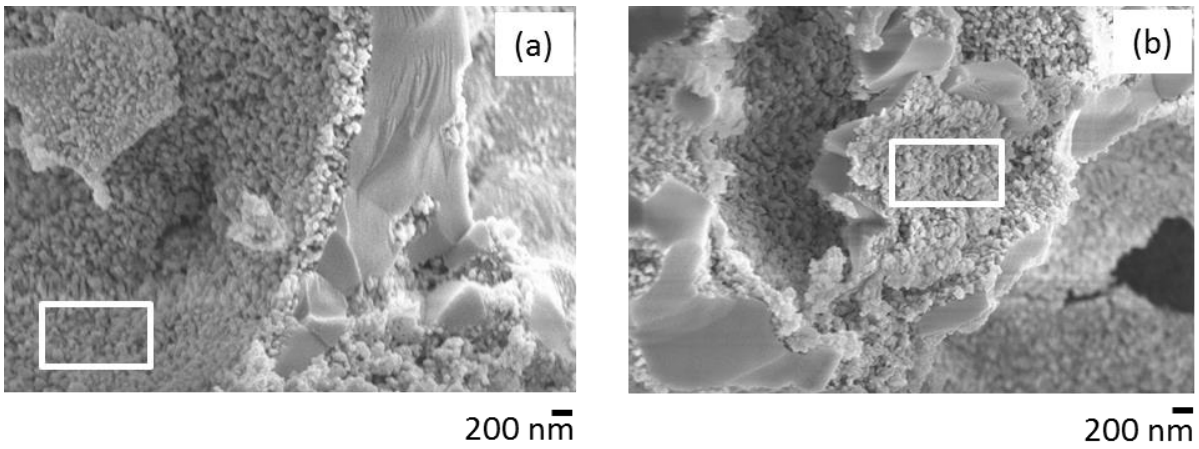

Figure 5. Post-operation of anode microstructure. SEM cross section images of the 2xNi-$SDCN_{40}$ anode after operation with: (a) 3% humidified hydrogen and (b) ethanol-water blend. The labeled anode catalyst regions within the porous SCSZ backbone were analyzed via EDS.

Conclusions

We have implemented a methodical study to deconvolute hydrogen concentration and catalytic reforming effects in SOFCs when operating with internal reforming of ethanol fuel. Hydrogen, simulated reformate, and hydrogen-nitrogen mixtures were used to obtain fundamental insight into the major limitations of internal reforming. With the exception of this work and a few other literature reports, severely limited performance when reforming ethanol is observed throughout the literature. This suggests the necessity for a direct performance comparison between simulated reformate (externally fully reformed ethanol, or custom gas mixture which corresponds to full internal reforming and equilibrium gas composition expected from thermodynamic calculations) and ethanol fuel to isolate the reforming limitation, rather than indirect comparison with hydrogen. Therefore, simulated ethanol reformate fuel should be considered as a standard baseline for internal reforming studies. Obtaining a fundamental understanding behind individual hydrogen concentration and reforming effects may lead to more accurate representation of the

internal reforming limitation in SOFCs. Therefore, a standard approach towards quantifying and predicting hydrogen concentration and reforming effects during internal reforming of ethanol seems necessary. Further evaluation of the detailed chemical reactions occurring in the gas phase and on the Ni surface throughout the active anode layer and anode-side metal support would also be useful.

Symmetric-architecture MS-SOFCs have been optimized for high performance and longevity with internal reforming of ethanol fuel. Performance of baseline MS-SOFC was determined to be limited by both hydrogen concentration and internal reforming. Addition of extra Ni to the MS-SOFC anode resulted in excellent performance in the presence of internal reforming, and the remaining decrease in peak power density, when compared to hydrogen fuel, was attributed solely to decrease in hydrogen concentration. Simple infiltration of high-surface area Ni nanoparticles over the fuel-side metal support and anode layers lead to unprecedented peak power density between 1.0 – 1.4 W cm^{-2} at 650 - 700 °C, with internal reforming of ethanol-water bend and anhydrous ethanol fuel. Stable electrochemical operation in ethanol-water blend was observed after 25 hours at 700 °C and 0.7 V. The post-mortem SEM and EDS analysis showed absence of coking on 2xNi-$SDCN_{40}$ anode.

Acknowledgments

The information, data, or work presented herein was funded in part by the Advanced Research Projects Agency – Energy (ARPA-E), U.S. Department of Energy under work authorization numbers 13/CJ000/04/03 and 18/CJ000/04/01. This work was funded in part by the U.S.

Department of Energy under contract no. DE-AC02-05CH11231. We thank Nissan Motor Co., Ltd. and Nissan Technical Center North America for providing cost share and helpful discussion.

Work at the Molecular Foundry was supported by the Office of Science, Office of Basic Energy Sciences, of the U.S. Department of Energy under Contract No. DE-AC02-05CH11231.

References

[1] M. Cimenti, J.M. Hill, Energies, 2 (2009) 377-410.
[2] S. C. Singhal, Solid State Ionics, 152 (2002) 405-410.
[3] S. C. Singhal, K. Kendall, High Temperature Solid Oxide Fuel Cells - Fundamentals, Design and Application, 1st ed., Elsevier, Oxford, U.K., 2003.
[4] A. M. Hussain, E. D. Wachsman, Energy Technology, 7 (2019) 20-32.
[5] B. C. Yang, J. Koo, J. W. Shin, D. Go, J. H. Shim, J. An, Energy Technology, 7 (2019) 5-19.
[6] W. Wang, J. F. Qu, P. S. B. Juliao, Z. P. Shao, Energy Technology, 7 (2019) 33-44.
[7] B. Zhu, Journal of Power Sources, 93 (2001) 82-86.
[8] M. C. Tucker, G. Y. Lau, C. P. Jacobson, L. C. DeJonghe, S. J. Visco, ECS Transactions, 7 (2007) 279-284.
[9] M.C. Tucker, Journal of Power Sources, 195 (2010) 4570-4582.
[10] M. C. Tucker, G. Y. Lau, C. P. Jacobson, L. C. DeJonghe, S. J. Visco, Journal of Power Sources, 171 (2007) 477-482.
[11] E. Dogdibegovic, R. Wang, G. Y. Lau, M. C. Tucker, Journal of Power Sources, 410 (2019) 91-98.
[12] M. C. Tucker, G. Y. Lau, C. P. Jacobson, L. C. DeJonghe, S. J. Visco, Journal of Power Sources, 175 (2008) 447-451.
[13] P. Blennow, J. Hjelm, T. Klemenso, S. Ramousse, A. Kromp, A. Leonide, A. Weber, Journal of Power Sources, 196 (2011) 7117-7125.

[14] T. Klemenso, J. Nielsen, P. Blennow, A. G. Persson, T. Stegk, P. Hjalmarsson, B. H. Cristense, S. Sonderby, J. Hjelm, and S. Ramousse, ECS Transactions, 35 (2011) 369-378.
[15] N. Christiansen, M. Wandel, S. Ramousse, and A. Hagen, ECS Transactions, 57 (2013) 43-52.
[16] V. V. Krishnan, Wiley Interdisciplinary Reviews-Energy and Environment, 6 (2017).
[17] Y. B. Matus, L. C. De Jonghe, C. P. Jacobson, S. J. Visco, Solid State Ionics, 176 (2005) 443-449.
[18] M.C. Tucker, International Journal of Hydrogen Energy, 43 (2018) 8991-8998.
[19] M.C. Tucker, Journal of Power Sources, 395 (2018) 314-317.
[20] Y. Jiang, A.V. Virkar, Journal of the Electrochemical Society, 148 (2001) A706-A709.
[21] H. J. Jeong, J.W. Kim, D. Y. Jang, J. H. Shim, Journal of Power Sources, 291 (2015) 239-245.
[22] W. Wang, F. Wang, R. Ran, H. J. Park, D. W. Jung, C. Kwak, Z. P. Shao, Journal of Power Sources, 265 (2014) 20-29.
[23] R. Peters, R. Dahl, U. Kluttgen, C. Palm, D. Stolten, Journal of Power Sources, 106 (2002) 238-244.
[24] C. M. Finnerty, R. M. Ormerod, Journal of Power Sources, 86 (2000) 390-394.
[25] I. A. Proctor, A. L. Hopkin, R. M. Ormerod, Ionics, 9 (2003) 242-247.
[26] J. A. Liu, S. A. Barnett, Solid State Ionics, 158 (2003) 11-16.
[27] A. L. Lee, R. F. Zabransky, W. J. Huber, Industrial & Engineering Chemistry Research, 29 (1990) 766-773.
[28] J. M. Klein, M. Henault, P. Gelin, Y. Bultel, S. Georges, Electrochemical and Solid State Letters, 11 (2008) B144-B147.
[29] N. Sammes, L. Varadaraj, Denki Kagaku, 63 (1995) 41-46.
[30] D. J. L. Brett, A. Atkinson, D. Cumming, E. Ramirez-Cabrera, R. Rudkin, N. P. Brandon, Chemical Engineering Science, 60 (2005) 5649-5662.
[31] T. Kim, K. Ahn, J. M. Vohs, R. J. Gorte, Journal of Power Sources, 164 (2007) 42-48.
[32] B. Zhu, X. G. Liu, P. Zhou, X. T. Yang, Z. G. Zhu, W. Zhu, Electrochemistry Communications, 3 (2001) 566-571.
[33] K. Sasaki, K. Watanabe, Y. Teraoka, Journal of the Electrochemical Society, 151 (2004) A965-A970.
[34] B. Huang, S. R. Wang, R. Z. Liu, X. E. Ye, H. W. Nie, X. E. Sun, T. L. Wen, Journal of Power Sources, 167 (2007) 39-46.
[35] X. F. Ye, B. Huang, S.R. Wang, Z.R. Wang, L. Xiong, T. L. Wen, Journal of Power Sources, 164 (2007) 203-209.
[36] B. Huang, S. R. Wang, R. Z. Liu, T. L. Wen, Journal of Power Sources, 167 (2007) 288-294.
[37] M. Cimenti, J. M. Hill, Asia-Pacific Journal of Chemical Engineering, 4 (2009) 45-54.
[38] Z. L. Zhan, S. A. Barnett, Science, 308 (2005) 844-847.
[39] M. F. Liu, Y. M. Choi, L. Yang, K. Blinn, W. T. Qin, P. Liu, M. L. Liu, Nano Energy, 1 (2012) 448-455.
[40] S. Diethelm, J. Van herle, Journal of Power Sources, 196 (2011) 7355-7362.
[41] E. N. Armstrong, J. W. Park, N. Q. Minh, Electrochemical and Solid State Letters, 15 (2012) B75-B77.
[42] B. L. Augusto, F. B. Noronha, F. C. Fonseca, F. N. Tabuti, R. C. Colman, L. V. Mattos, International Journal of Hydrogen Energy, 39 (2014) 11196-11209.

[43] H. Sumi, T. Yamaguchi, H. Shimada, Y. Fujishiro, M. Awano, Fuel Cells, 17 (2017) 875-881.
[44] M. C. Steil, S. D. Nobrega, S. Georges, P. Gelin, S. Uhlenbruck, F.C. Fonseca, Applied Energy, 199 (2017) 180-186.
[45] A.A.A. da Silva, N. Bion, F. Epron, S. Baraka, F.C. Fonseca, R. C. Rabelo-Neto, L. V. Mattos, F. B. Noronha, Applied Catalysis B-Environmental, 206 (2017) 626-641.
[46] M. M. Liao, W. Wang, R. Ran, Z.P. Shao, Journal of Power Sources, 196 (2011) 6177-6185.
[47] W. Wang, Y. B. Chen, F. Wang, M. O. Tade, Z. P. Shao, Chemical Engineering Science, 126 (2015) 22-31.
[48] M. Lo Faro, R. M. Reis, G. G. A. Saglietti, V. L. Oliveira, S.C. Zignani, S. Trocino, S. Maisano, E. A. Ticianelli, N. Hodnik, F. Ruiz-Zepeda, A.S. Arico, Applied Catalysis B-Environmental, 220 (2018) 98-110.
[49] S. D. Nobrega, P. Gelin, S. Georges, M.C. Steil, B.L. Augusto, F.B. Noronha, F.C. Fonseca, Journal of the Electrochemical Society, 161 (2014) F354-F359.
[50] X. F. Ye, S. R. Wang, Q. Hu, J. Y. Chen, T. L. Wen, Z. Y. Wen, Solid State Ionics, 180 (2009) 276-281.
[51] X. F. Ye, S. R. Wang, Q. Hu, Z. R. Wang, T. L. Wen, Z.Y. Wen, Electrochemistry Communications, 11 (2009) 823-826.
[52] X. F. Ye, J. Zhou, S. R. Wang, F. R. Zeng, T. L. Wen, Z. L. Zhan, International Journal of Hydrogen Energy, 37 (2012) 505-510.
[53] M. Cimenti, J.M. Hill, Journal of Power Sources, 195 (2010) 3996-4001.
[54] S. P. Jiang, Y. M. Ye, T. M. He, S. B. Ho, Journal of Power Sources, 185 (2008) 179-182.
[55] N. K. Monteiro, F. B. Noronha, L. O. O. da Costa, M. Linardi, F. C. Fonseca, International Journal of Hydrogen Energy, 37 (2012) 9816-9829.
[56] B. Farrell, S. Linic, Applied Catalysis B-Environmental, 183 (2016) 386-393.
[57] C. Resini, M. C. H. Delgado, S. Presto, L. J. Alemany, P. Riani, R. Marazza, G. Ramis, G. Busca, International Journal of Hydrogen Energy, 33 (2008) 3728-3735.
[58] M. Morales, F. Espiell, M. Segarra, Journal of Power Sources, 293 (2015) 366-372.
[59] M.C. Tucker, Energy Technology, 5 (2017) 2175-2181.
[60] WebPlotDigitizer, https://automeris.io/WebPlotDigitizer, (accessed on June 25, 2019).
[61] E.B. C. W. Bale, Equilib-Web Software, http://www.crct.polymtl.ca/equiweb.php (accessed on May 25, 2019).
[62] P. Leone, A. Lanzini, G.A. Ortigoza-Villalba, R. Borchiellini, Chemical Engineering Journal, 191 (2012) 349-355.
[63] A. Hagen, X. Sun, B. R. Sudireddy, A. H. Persson, Electrochemical Transactions, 91(1) (2019) 867-876.
[64] E. Dogdibegovic, R. Wang, G. Y. Lau, A. Karimaghaloo, M. H. Lee, M. C. Tucker, Journal of Power sources, 437 (2019), 226935.
[65] E. C. C. Souza, W. C. Chueh, W. Jung, E. N. S. Muccillo, S. M. Haile, Journal of the Electrochemical Society, 159 (2012) K127-K135.
[66] W. Wang, C. Su, R. Ran, B. T. Zhao, Z. P. Shao, M. O. Tade, S. M. Liu, Chemsuschem, 7 (2014) 1719-1728.
[67] X. F. Ye, S. R. Wang, Z. R. Wang, L. Xiong, X. E. Sun, T.L. Wen, Journal of Power Sources, 177 (2008) 419-425.

[68] X. F. Ye, S. R. Wang, Z. R. Wang, Q. Hu, X. F. Sun, T. L. Wen, Z. Y. Wen, Journal of Power Sources, 183 (2008) 512-517.